COURSE 1

MELTING OF CLUSTERS

HELLMUT HABERLAND

Fakultät für Physik, Universität Freiburg, H.Herderstr. 3, D-79104 Freiburg, Germany

Version as of May 17, 2001

Contents

1 Introduction **3**

2 Cluster Calorimetry **4**
2.1 The bulk limit 5
2.2 Calorimetry for free clusters 7

3 Experiment **8**
3.1 The source for thermalized cluster ions 10

4 Caloric Curves **11**
4.1 Melting temperatures 12
4.2 Latent heats 14
4.3 Other experiments measuring thermal properties of free clusters . . 15

5 A closer look on the experiment **16**
5.1 Beam Preparation 16
5.1.1 Reminder: Canonical versus Microcanonical Ensemble . . . 16
5.1.2 A canonical distribution of initial energies 16
5.1.3 Free clusters in vacuum, a microcanonical ensemble 17
5.2 Analysis of the fragmentation process 17
5.2.1 Photo excitation and energy relaxation 17
5.2.2 Mapping of the energy on the mass scale 18
5.2.3 Broadening of the mass spectra due to the statistics of evaporation 19
5.3 Canonical or microcanonical data evaluation 20

6 Results obtained from the closer look **21**
6.1 Negative heat capacity 21
6.2 Entropy 23

7 Unsolved problems **24**

8 Summary and Outlook **25**

9 Acknowledgement **26**

MELTING OF CLUSTERS

Hellmut Haberland

Abstract

An experiment is described which allows to measure the caloric curve of size selected sodium cluster ions. This allows to determine rather easily the melting temperatures, and latent heats in the size range between 55 and 340 atoms per cluster. A more detailed analysis is necessary to show that the cluster Na_{147}^{+} has a negative microcanonical heat capacity, and how to determine the entropy of the cluster from the data.

1 Introduction

Melting in a macroscopic object occurs at some well defined temperature. This is no longer true for a small particle or cluster. If one talks about melting one must first verify whether the concepts of *solid* or *liquid* can be transferred to small systems. The answer is yes: at low temperatures the atoms in a cluster or in a large piece of matter make only small amplitude vibrations around a fixed position. It takes a lot of energy to push an atom from its position and one has a solid. If the temperature increases, atoms in the cluster can visit neighbouring places and start a diffusive motion. There is very little resistance to external deformation forces and the cluster is liquid. This is demonstrated in Fig. 1 which shows a simulation for a cold, rigid and a liquid, hot cluster. The simulation was done with the potential parameters for argon. But the main features of small harmonic oscillations at low and more diffusive motion at high temperatures are independent of the force field assumed.

Concepts like temperature, phase etc. had originally been defined only for infinitely large systems. But one has learned how to generalize these concepts to finite particles, although there are still some more semantic quarrels about nomenclature. For the solid to liquid transition of finite systems one finds four main differences with respect to the bulk counterpart, 1) the

The work was supported by the Deutsche Forschungsgemeinschaft through SFB 276.

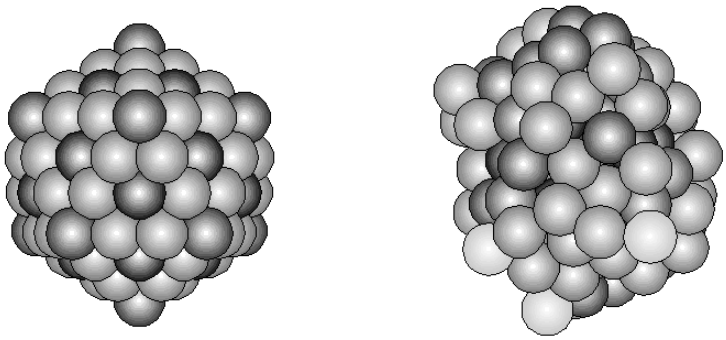

Fig. 1. A simulation of a cluster of 147 atoms at T = 0 K (left figure) and a high temperature. The darker the colour, the more strongly an atom is bound. The calculation was made using a Lennard–Jones potential, which is not adequate for the sodium clusters discussed in this report. So one does not know whether the low temperature structure of Na_{147}^{+} really looks like this icosahedron, whose regular, five fold symmetry can be well seen here. The general features of the solid to liquid transition however, should be independent of the force field assumed. (Calculation by Michael Moseler, colour pictures on the WEB site of the author.)

melting point is generally reduced (part 4.1), 2) the latent heat is smaller (part 4.2), and 3) the transition does not occur at one definite temperature but is spread out over a temperature range. The fourth difference is quite spectacular: the heat capacity can become negative, i.e. the temperature of the system can decrease upon energy addition (part 6.1).

Experimentally, the depression of the melting point has been shown [1] as early as 1908. Many experiments have been done with particles on surfaces which contained thousands or millions of atoms [2]. Also, very many computer simulations have been performed to get a better understanding [3–6]. They have shown how the bulk concepts like temperature and melting can be generalized to finite systems. Nearly all simulations have been performed for free clusters of known size, while most earlier experiments have been performed with particles on surfaces having a rather broad size distribution.

2 Cluster Calorimetry

All experiments to study the melting point of bulk material or of clusters can be divided into two classes.

1. One studies the change of some physical property across the melting point, e.g. change in photon or X–ray diffraction patterns, or mobility.

2. The caloric curve $E = E(T)$ is measured, that is the clusters internal energy E as a function of its temperature T. This curve contains all the thermodynamic information, as discussed below.

The experiment discussed here, is of the second type. It measures the caloric curve $E = E(T)$ for free sodium cluster ions, where the number of atoms is exactly known.

2.1 The bulk limit

It is often very useful in cluster science to study the asymptotic behaviour, that is that of the atom and that of the bulk. Although there is a well understood bulk limit, the atom and the diatomic molecule do obviously not have a melting point. It seems that at least seven atoms are needed before something like a liquid behaviour is seen in numerical simulations.

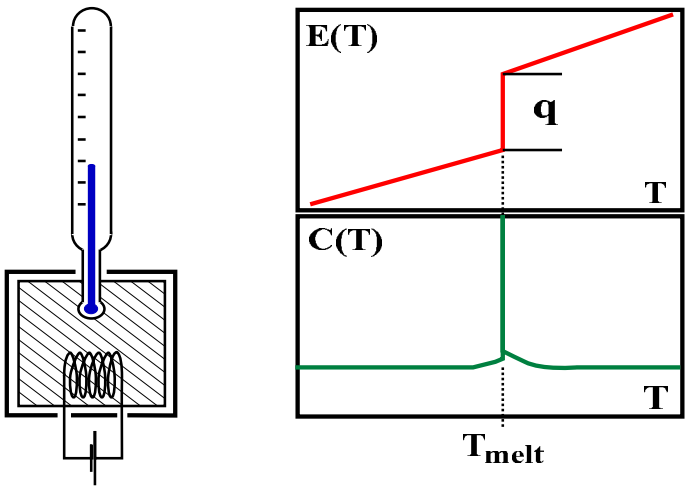

Fig. 2. Calorimeter (left), caloric curve $E = E(T)$ and heat capacity $C(T)$ for a macroscopic sample. The caloric curve increases abruptly at the sharp melting temperature (T_{melt}). The height of the jump is given by the latent heat q of melting. The heat capacity has a delta function like peak at T_{melt} (see Eq. 2.1.)

It is in principle easy to measure the caloric curve for bulk materials. One puts the material into a thermally isolated container (see Fig. 2), adds energy E and measures the temperature T. After compensation for the thermal mass of the container, one can construct the caloric curve, $T = T(E)$, or $E = E(T)$.

For a large system, the caloric curve exhibits a step at the melting temperature T_{melt}. The height of the step is the latent heat q. Energy can be added to the system at T_{melt} without an increase of temperature; all the energy is used to destroy the regular solid structure, and thus increase the entropy. This fact is widely used when drinks are cooled by ice cubes. The large latent heat of ice makes it an efficient coolant. Only when the system has become completely liquid, the temperature will rise again upon addition of energy. Note, that one has phase separation for a large sample, i.e. water and ice coexist together at T_{melt}. As discussed below (part 6.1), phase separation is not possible for a sufficiently small system. The derivative of the

Fig. 3. One would like to make an experiment as shown here, which would be the direct generalization of the setup in Fig. 2 to free clusters. Energy is supplied, here by a candle, in an experiment more probably by a laser. The temperature is measured by a thermometer, which could be a small molecule, whose states are interrogated by another laser. This method of temperature measurement has been studied but no reliable temperature scale could be established so far.

caloric curve is called the heat capacity $C(T)$ or also the specific heat [7]:

$$C(E) = \frac{\partial E(T)}{\partial T} \tag{2.1}$$

It has a delta function like peak at the melting temperature for a bulk system.

It is possible today to construct "nano–calorimeters" using the techniques of the semiconductor chip industry, which carry the principle of Fig. 2 to very small particles. In the year 2000 the lower limit of this technique is a particle size of about 1000 atoms [8]. Also electron and X–ray diffraction has been used to study clusters deposited on surfaces [8]. At present these methods are however not applicable to free, mass selected clusters in vacuum for two reasons: First no method of temperature measurement is known in this case, and also the density of mass selected clusters is so small, that it near to impossible to collect a diffraction signal. Earlier attempts to circumvent this problem can be found in ref. [9–13]. An experiment on electron diffraction on stored cluster ions has recently been published [32], which opens the possibility of doing a type 1 experiment on stored, thermalized ions.

2.2 Calorimetry for free clusters

The thermal experiments on free, mass selected clusters have only been performed with sodium so far. Sodium has been chosen for two reasons: 1) It was the aim of this experiment to work with mass selected clusters, i.e. the number of atoms in the cluster is exactly known. In this case one has to use a mass spectrometer, which forces one to work with ions. For non–metallic elements their can be quite a difference between the electronic and geometric structure of a neutral and a positively charged cluster [33]. Due to the delocalized nature of the chemical bond this is not the case in metals. 2) From all the metals available, sodium is the easiest to calculate.

The cluster calorimetry [14–19] method developed in our group does the inverse of the bulk method shown in Figs. 2 and 3. Size selected clusters of known temperature are prepared and their energy (more exactly their energy distribution, averaged over an experimental broadening) is measured. The method consists essentially of two steps, as indicated in Fig. 4.

Step 1 *Preparation of size selected cluster of known temperature.* Cluster ions are produced and thermalized in a heat bath. A mass spectrometer is used to select a single cluster size. This prepares clusters of known size and known temperature T.

Step 2 *Determination of their energy.* The clusters are irradiated by a laser beam and absorb several photons. This leads to the evaporation of

atoms. A second mass spectrometer measures the distribution of the fragment ions produced, which has a characteristic shape as shown in Fig. 5. Different numbers of absorbed photons lead to clearly separated groups of fragments in the mass spectrum, with the distance between two groups corresponding to exactly one photon energy. This allows one to calibrate the mass scale in terms of energy [14–17].

If the temperature of the heat bath is varied, the inner energy of the selected cluster changes and thus also the number of evaporated atoms. The fragment groups shift on the mass scale as shown in the inset of Fig. 5. These twodimensional plots are the primary data of the experiment. From them the caloric curve $E = E(T)$ can be determined directly as indicated in the figure. This method of data treatment has several advantages compared to the one used earlier [14–16]; it is more robust, and avoids the averaging inherent in the use of the finite difference approximation to Eq. 2.1 used earlier (Eq. 4 of ref. [14]).

3 Experiment

The schematic of the experiment is shown in Fig. 4. In more detail, two Time–Of–Flight (TOF) mass spectrometers of the reflectron type are used in tandem. The detector is an Even cup [20] employing up to 30 kV post acceleration for efficient detection of the heavier clusters. The fragmentation laser is an excimer pumped dye laser. The experimental setup is similar to those used by other groups. The novel and at the same time crucial part of

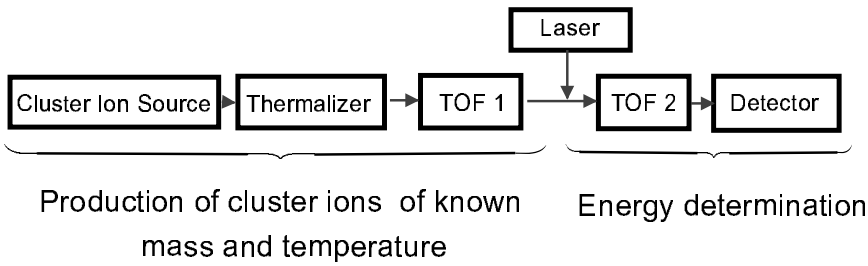

Fig. 4. Schematic of the experiment. Cluster ions are produced and thermalized in a heat bath of known temperature T. A first time of flight mass spectrometer (TOF 1) selects one cluster size. In this way, a cluster of known temperature and known mass is produced (see Step 1 above). The clusters absorb several photons from a pulsed laser, and the distribution of the charged fragments is measured by TOF 2. From these data the energy E before irradiation can be determined, as explained in Fig. 5. When energy and temperature are known, the caloric curve $E = E(T)$ can be constructed (Step 2 above).

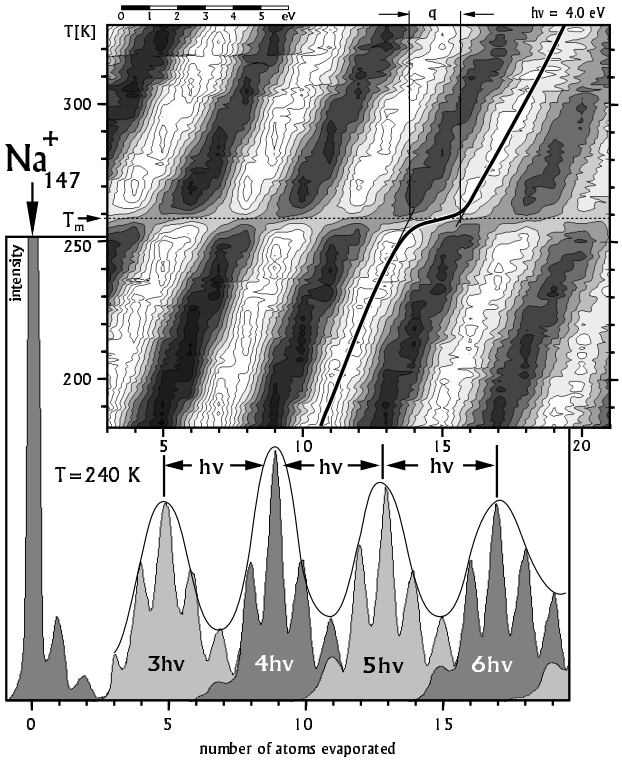

Fig. 5. The energy E of a free cluster can be obtained from its photofragmentation mass spectrum. In the experiment, a Na^+_{147} cluster is prepared at a temperature of 240 K. After absorption of several photons the cluster starts to emit neutral atoms. The intensity of the remaining charged fragments is plotted against the number of evaporated atoms (lower panel). Without laser one observes only the large peak on the left, corresponding to the intact Na^+_{147}. For four absorbed photons one has an approximately Gaussian distribution of photofragments centered around nine evaporated atoms. For five (six) absorbed photons the Gaussian is centered near thirteen (seventeen) ejected atoms. The distance between the maxima of the Gaussians corresponds to exactly one photon energy, which allows an energy calibration of the mass scale. As for all calorimeters, energy calibration is only good up to an additional constant.

Inset: The mass peaks are connected by a smooth function, and plotted against the temperature of the thermalization cell of Fig. 4 and 6. White implies high intensity. The caloric curve is obtained by connecting the maxima; one example is shown. The other maxima are just shifted by the photon energy. The melting temperature is indicated at the left and the latent heat q at the top. Note, that the lower panel is for 240 K, while the inset is for 180 to 330 K.

the experiment is the source for thermalized cluster ions.

3.1 The source for thermalized cluster ions

The source is shown in Fig. 6. It consist of two main parts, the cluster source itself (left part) and the thermalization stage. In the source, sodium is evaporated into a cold, slowly streaming helium gas of about 70 Pa. Mostly sodium atoms and a few dimers leave the boiling liquid, which aggregate in the cold He gas to clusters. The He gas can be added at two points, one at the far side of the aggregation tube, or it can be directly blown into the sodium container. One can optimize the intensity by varying the relative gas flow through the two inlets. A weak electric gas discharge (∼100V, about 1 mA) is ignited with the sodium container working as a hollow cathode. This leads to an efficient production of positively charged sodium cluster ions. Probably, charged molecular dimers, like Na_2^+ or He_2^+ act as condensation germs. Once a dimer is built, cluster formation starts rapidly. The process is similar to cloud formation in nature and will not be discussed here.

The tube containing the aggregation zone has a diameter of about 10 cm.

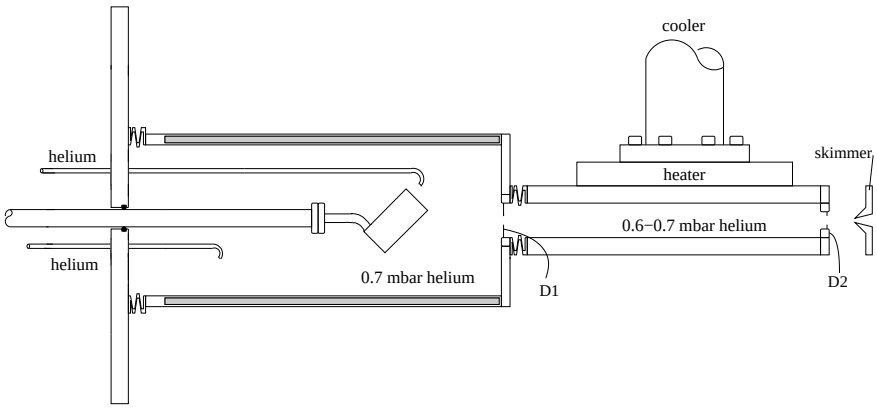

Fig. 6. The gas aggregation source used to produce thermalized cluster ions. Sodium is evaporated from a small, tilted container into a cold stream of He gas. A gas discharge (not shown) is ignited and produces charged species. Aggregation is very effective up to diaphragm D1. The cluster formation stops effectively after D1 due to the low density of sodium atoms there. The helium gas transports the clusters from the source region (left) through D1 into the thermalization region. There they make 10^5 to 10^6 collisions with He atoms, whose temperature T can be adjusted by a heater/cooler. The cluster acquire a *canonical* distribution of energies at the temperature T.

It is cooled by liquid nitrogen, which facilitates the production of smaller clusters, and also leads to a more stable operation. The clusters together with the helium gas leave the aggregation zone through a diaphragm (D1) of variable diameter, which is an iris aperture normally used in optics. The clusters enter a copper tube, which can be cooled down to 30 K and heated up to 600 K. They leave this tube through a second variable iris (D2). Most of the helium is pumped away, and the clusters continue to fly through a skimmer into the first mass spectrometer. Both irises and the skimmer are electrically isolated and carry a small potential (less than 10 V) to compensate for surface charges and plasma effects.

The setup with the both adjustable irises is mechanically somewhat complicated, but at least the diameter of iris D2 must be adjustable during the experiment if one wants to scan over a sufficiently large temperature range. The viscosity of a gas scales as $T^{-1/2}$ and the gas flux through small holes thus diminishes with increasing temperature. The cluster intensity is a sensitive function of the gas flux, and typically every 30 K the otherwise automatic measuring process has to be interrupted in order to optimize the beam intensity by adjusting iris and gas flow.

4 Caloric Curves

The primary results of the experiment are two–dimensional data fields as shown in Fig. 5. One obtains the caloric curve by connecting the maxima of the fragment distributions. Fig. 7 shows an example. A more detailed analysis of what is actually measured is given below (part 5.3).

At low temperatures, the caloric curve increases roughly linearly, and then shows a change in slope which is due to the melting process. Near the melting temperature a relative large amount of energy is needed for a small increase of temperature. The sudden jump of bulk systems is smoothed to a finite width. The melting temperature is indicated. The latent heat q is equal to the increase in the caloric curve near T_{melt}. For higher temperatures, a nearly linear increase is again observed. The following data can be read off Fig. 7: 1) the melting temperature T_{melt} as given in Fig. 8, 2) the latent heat given in Fig. 9, and 3) more generally, the specific heat as a function of temperature. In the temperature range studied, the heat capacity (the derivative of the caloric curve with respect to the temperature) is nearly constant below and above T_{melt}. It is generally higher above T_{melt}. For smaller cluster sizes, melting temperature and latent heat diminish. We have measured several caloric curves, (e.g. Na^+_{70} and Na^+_{93}) where there seems to be only a bend (and not a smoothed out step) in the caloric curves. Data from these curves are not included below.

At a temperature above 400 K, the clusters are so hot that they can evaporate atoms without having absorbed a photon. Thus they are no

longer thermalized when they arrive in the laser interaction zone. Therefore the very high temperature part of the curve does not belong to the caloric curve, but describes an evaporative ensemble [21], whose temperature and energy can be read off Fig. 7.

From the discussion below (part 5.3), it will become apparent that Fig. 7 does show for temperatures below 400 K a microcanonical caloric curve, but averaged over the unavoidable broadening due to the photofragmentation process. Therefore a possible backbending cannot be seen, and the curve looks like a canonical one. Outside $T_{melt} \pm$ 20K canonical and microcanonical curves agree within experimental error.

4.1 Melting temperatures

The temperature corresponding to the of largest slope of the caloric curve is identified as the melting point. The data available so far are shown in

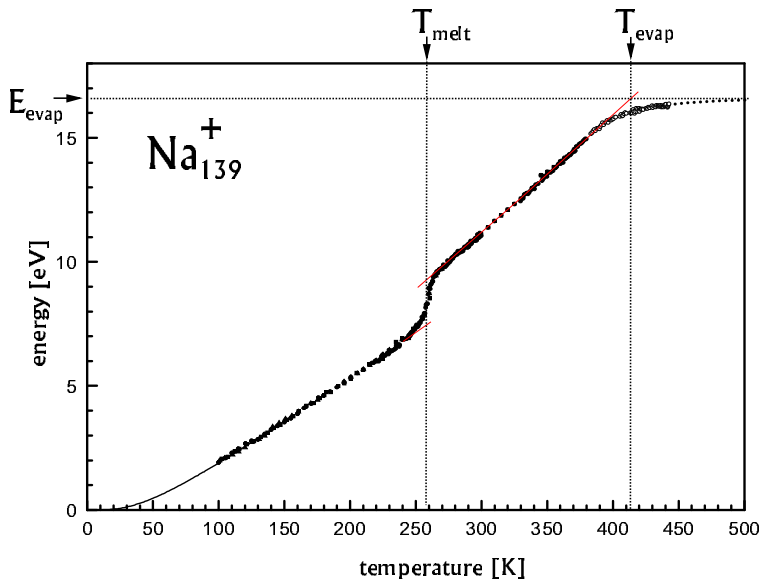

Fig. 7. Caloric curve for Na^+_{139} . Below 100 K the curve has been extrapolated using the bulk result. The soft increase near 260 K is due to the melting process. Melting temperature and latent heat can be easily read off the curve. Above 400 K the data deviate from the caloric curve as the cluster can no longer be thermalized.

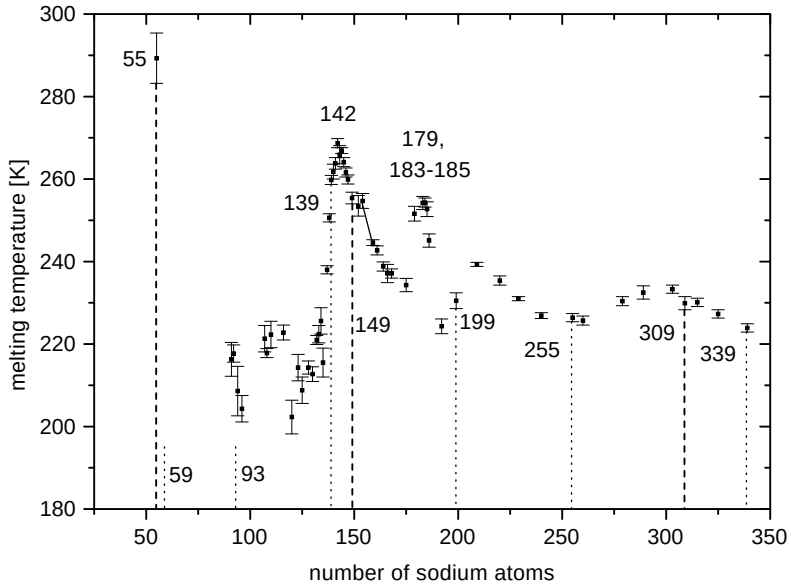

Fig. 8. The melting temperatures of Na_n^+ are plotted against the number of atoms. Large fluctuations are seen whose origin is not well understood. They do not correlate with electronic (dotted line) or geometric (dashed) shell closings, which are indicated in the figure. The bulk melting temperature is 371 K. Note, that the zero is suppressed.

Fig. 8. The melting points show surprisingly large variations: one additional atom can change T_{melt} by up to 10 K. Two main points can be observed: 1) the melting temperatures are about one third lower than in the bulk, and 2) they fluctuate by $\pm$ 50 K. From less complete data it had earlier been conjectured that the melting points are high, if electronic and geometric shell closings are close to each other. This is no longer supported by the new data covering a wider mass range.

Several calculations [6, 22–25] have been performed on melting of sodium clusters, but the overall structure of the data in Fig. 8 has not been reproduced so far. The number of atoms for the maxima and minima in Fig. 8 do not generally correspond to any known shell closings, be they electronic or atomic in origin. Also, it might be that the cluster changes its geometry near the melting temperature, as has been observed in a simulation on gold clusters [5].

Many calculated melting temperatures for a variety of cluster sizes with

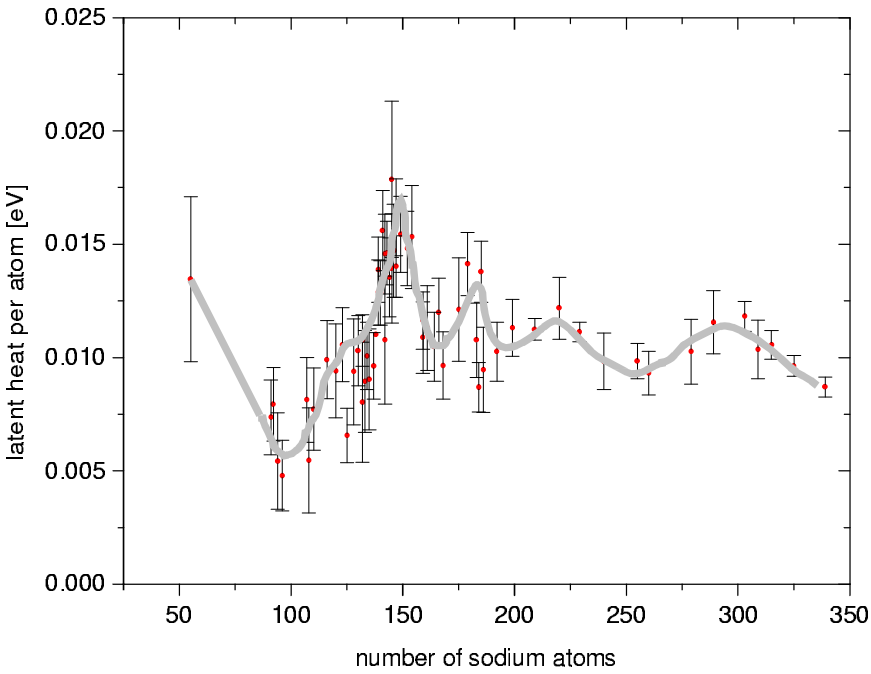

Fig. 9. The latent heat per atom is plotted against the number of atoms in the cluster. Large fluctuations are visible which correlate with those of the melting point. The line through the data is only drawn to guide the eye. The bulk value is 27.5 meV.

less than 30 atoms show a surprisingly simple scaling with the parameter $S = \overline{E}_{int}/\overline{E}_{sur}$, where $\overline{E}_{int}$ and $\overline{E}_{sur}$ are the mean potential energies of the internal atoms and the surrounding atoms, respectively [26]. It would be interesting to see if the larger clusters studied here behave similarly.

For two cluster sizes (70 and 93 atoms) the caloric curve does not show an increase like in Fig. 7, but only a bend, which can be either interpreted as melting with a very small latent heat, or as the lower temperature of an extended melting range. No upper range is found in the data until the clusters evaporate at 400 and 410 K, respectively. These data are not included in Fig. 8.

4.2 Latent heats

Classically, the latent heat is the energy to destroy the lattice at the melting temperature. Here it is measured as indicated in Figs. 5 and 7 as the height of the increase of the caloric curve near T_{melt}. The vertical scale in Fig. 7 is

energy calibrated, so that the latent heats are obtained absolutely. The data are more noisy than those in Fig. 8, but they seem to indicate a correlation of the extrema with those of the melting points, at least for the data above n = 100. This correlation is physically plausible as the higher the melting point, the more the crystal lattice can withstand thermal energy, i.e. the higher the latent heat.

4.3 Other experiments measuring thermal properties of free clusters

There is quite a history of earlier experiments trying to measure the melting behaviour of free cluster. The groups of Buck [9], Even/Jortner [10] looked for spectroscopic evidence. Electron diffraction from a not mass selected supersonic expansion gives Debye–Scherrer like diffraction rings, the intensity of them being a measure of cluster temperature. This was pioneered by the Farges/Torchet group [27] and later intensively studied Bartell et al. [12].

The T.P.Martin group [11] were the first to publish a size dependence of the melting temperatures of free clusters. They showed that the structure on mass spectra of large sodium clusters depends sensitively on the temperature, if the photon energy is chosen appropriately. The disappearance of the structure was interpreted as being due to melting.

Another method has been used to measure melting temperatures of free clusters. It has been applied to small tin clusters with the surprising result that their melting point is higher than the bulk one [28]. In this experiment, cluster ions are injected into a helium gas, and are pulled by an electric field through the gas. They make very many collisions, which produces an effective friction force. Clusters having a small collision cross section make fewer collisions, thus experience a smaller friction force and arrive first. Small Sn–clusters have a rather elongated structure which should change to near spherical upon melting . A change in collision cross section can thus be expected upon melting. No signature of melting is observed, so that the authors conclude that tin cluster ions containing 10 to 30 atoms have a melting point which is at least 50 K above the bulk one [28, 29].

The experiments discussed above all belong to class 1, as defined in the introduction to chapter 2, i.e. some physical property (optical or mass spectrum, diffusion cross section ...) is studied as a function of temperature. The only other experiment belonging to class 2, has been used to measure caloric curves of free tin clusters [30]. These were produced by a laser ablation source using a pulsed nozzle whose temperature is variable. The authors estimate that nozzle and cluster temperature deviate by 10 to 20 K only. Neutral clusters are studied so that no mass selector can be used. The distribution of cluster sizes is not given, but similar experiments give a δm/m not smaller than 60%. The energy is measured very differently. The cluster impinge on a sensitive pyroelectric foil, whose temperature increase leads to a measurable voltage jump. The measured caloric curve looks very

similar to the one given in Fig. 7. Only the solid/liquid transition region is broader due to the cluster size distribution. The interpretation of the experiment has been questioned [31].

5 A closer look on the experiment

It was discussed above how caloric curves, melting points and latent heats can be directly obtained from the temperature dependence of the mass spectra. Here we will take a closer look at the experiment and analyse it in more detail. This is necessary, first to understand better what kind of experiment is actually performed, and second to extract more detailed information from the data.

5.1 Beam Preparation

Cluster ions are produced and thermalized in a heat bath, which gives them a canonical distribution of inner energies. For the further discussion, some definitions of basic Thermodyanmics are needed, which are briefly reviewed.

5.1.1 Reminder: Canonical versus Microcanonical Ensemble

In the theory of Thermodynamics one defines several idealized situations, called ensembles, which are particular important or easy to calculate [34]. Two of them are realized in this experiment. In the *canonical* ensemble one has a collection of physical systems (atoms, molecules, clusters, spins ...) which have a fixed temperature and a thermal distribution of energies. A physical realization are particles in contact with a large heat bath.

In a *microcanonical* ensemble on the other hand, the energy is fixed. A physical realization is an isolated particle in vacuum, which can neither emit nor absorb photons or atoms. Only for an infinitely large system the two ensembles give the same result, for a finite system there can be differences [4,6,35,36] which will be particular important near phase transitions.

5.1.2 A canonical distribution of initial energies

In the thermalizer of Fig. 4 and 6 the helium gas is in contact with the metal tube whose temperature is kept constant. Helium is a good heat conductor at the pressure of about 70 Pa. The He atoms are thermalized at the tube wall and in turn thermalize the clusters by collisions. The clusters make typically 10^5 to 10^6 collisions with the gas, more than sufficient for complete thermalization. Thus each cluster can be considered as a small system in contact with a large heat bath, and thus corresponds to a canonical ensemble. Theory tell us that in this case the small system has a *canonical*

distribution of energies $P_T(E)$, which is given by the density of states of the cluster $\Omega(E) = \exp\{S(E)/k_B\}$ times the Boltzmann factor [34].

$$P_T(E) \propto \Omega(E) \exp\{-E/k_B T\} = \exp\{S(E)/k_B - E/k_B T\} \qquad (5.1)$$

where $S(E) = k_B \ln \Omega(E)$ is the entropy, and k_B is Boltzmann's constant. The inset to Fig. 10 shows an example for $P_T(E)$; far from the melting temperature it is nearly Gaussian, near a phase transition $P_T(E)$ can become bimodal as seen in Fig. 11b. Eq. 5.1 is quite powerful, as it gives a relation between temperature, energy and entropy. One can, for example, take the measured caloric curve $E = E(T)$, plug it into Eq. 5.1, and obtain entropy and $P_T(E)$.

5.1.3 Free clusters in vacuum, a microcanonical ensemble

High vacuum is needed to operate a mass spectrometer, so that the clusters have to be transferred to a low pressure for mass selection. The aim of the experiment is to measure $P_T(E)$. Thus the cluster should not make any collisions between the thermalizer and the laser interaction zone which could alter this distribution. Care is taken to ensure this as far as possible, e.g. all nets, safe one, are removed from the ion flight path and the background pressure is kept sufficiently low. Then the energy of each *single* cluster stays effectively constant after it has left the heat bath, and one has a microcanonical ensemble. Averaging over many clusters, one regains $P_T(E)$ of Eq. 5.1. The energy of a single cluster is a sample of this distribution.

5.2 Analysis of the fragmentation process

The second step of the experiment (see introduction to chapter 2 and Fig. 4) is to measure the energy E, more exactly the distribution $P_T(E)$ of Eq. 5.1. Photofragmentation is used for want of a better method. The processes involved will be discussed now.

5.2.1 Photo excitation and energy relaxation

After mass selection the cluster absorbs several photons of energy $h\nu$. The excimer pumped dye laser has a pulse length of about 10 ns, which is orders of magnitude longer than electron–electron and electron–vibrational relaxation times [37]. The photon induces an excitation of the plasmon type [38–41] which decays through a chain of processes according to the following scenario: The collective plasmon excitation decays into a single electron excitation, which produces through electron–electron collisions a hot electron gas. This is turn couples to the vibrations. Only after complete relaxation, the next photon is absorbed. As the photon energy is smaller than the energy needed to eject an electron, no electron ejection is

seen with a nanosecond laser under low fluence. Only if the time between the absorption of two photons becomes of the order of the electronic relaxation time, one observed electron emission. But even under these much more violent excitation, no fast emission of atoms can be observed [37].

5.2.2 Mapping of the energy on the mass scale

If n photons are absorbed, the internal energy $U(E)$ of the cluster becomes

$$U(E) = nh\nu + P_T(E) \quad . \tag{5.2}$$

The original distribution $P_T(E)$ is shifted by several finite steps of $h\nu$ to higher energies. Once the energy is sufficiently high, the cluster starts to evaporate atoms [42] on the time scale of this experiment. The more energy a cluster carries before photoexcitation, the more atoms it will evaporate afterwards. Thus, the mass distribution corresponding to a fixed number of

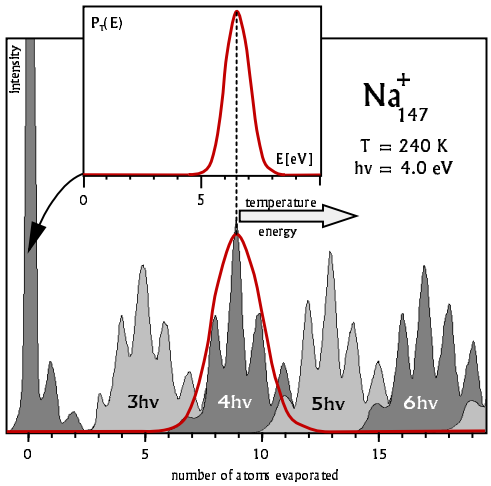

Fig. 10. Photofragmentation spectrum of Na^+_{147}. The intensity of each cluster ion is plotted against the number of atoms lost. Without laser one sees only the high peak at the left, whose distribution of inner energy $P_T(E)$ is given in the inset. The photon energy of $h\nu$ is more than four times the dissociation energy D_n so that the mass groups corresponding to a fixed number of absorbed photons are clearly separated. The mass peaks shift to the right with increasing temperature or photon energy, as indicated. The envelop of the mass peaks, indicated by the solid line, is the convolution of the initial thermal distribution $P_T(E)$ with the width $P_{evap}(E)$ due to the fragmentation process, as given by Eq. 5.6.

absorbed photons is a map of its internal energy distribution $U(E)$ as given by Eq. 5.2. The details of the mapping process are discussed in the caption to Fig. 10.

5.2.3 Broadening of the mass spectra due to the statistics of evaporation

The evaporation rate $k_n(E)$ is approximately given by

$$k_n(E) = \nu g \exp\{-sD_n/U(E)\} \tag{5.3}$$

Here ν is a typical frequency (10^{12} to 10^{13} Hz), $s = 3n-6$ is the number of vibrational degrees of freedom, g is a degeneracy factor usually taken as the number of surface atoms, and D_n is the dissociation energy of a cluster of n atoms. The time between laser excitation and ejection of the first atom is $t_n \approx k_n(E)^{-1}$, which decreases dramatically with increasing E. At each evaporation step

$$Na_n^+(E) \longrightarrow Na + Na_{n-1}^+(E - D_n - E_{kin}) + E_{kin} \tag{5.4}$$

the energy decreases by essentially the dissociation energy D_n. At each step of the fragmentation chain

$$Na_n^+ \xrightarrow{k_n} Na_{n-1}^+ \xrightarrow{k_{n-1}} Na_{n-2}^+ \xrightarrow{k_{n-2}} Na_{n-3}^+ \xrightarrow{k_{n-3}} Na_{n-4}^+ \cdots \tag{5.5}$$

the fragmentation rate decreases and the lifetime increases. Even if $P_T(E)$ was a δ–function, the mass distribution after the fragmentation has a finite width $P_{evap}(E)$ due to the statistical nature of the photofragmentation process. That is, more than one decay process can occur in the time window of the experiment; or in other words, the decay process described by k_{n-1} in Eq. 5.5 will start, before the k_n process is completed.

If the photon energy is sufficiently high (three to four times the energy needed to eject one atom from the cluster), the mass spectra $M_T(n)$ show an oscillatory structure as function of the number n of atoms evaporated, as shown in Fig. 5 and 10. The maxima and minima of the oscillations are exactly one photon energy apart, which allows an energy calibration of the mass scale. Thus one can transform $M_T(n)$ to $M_T(E)$. The envelope $M_T(E)$ of the energy–calibrated mass spectrum (see Fig. 10) becomes:

$$M_T(E) \propto P_T(E) \otimes P_{evap}(E) \quad , \tag{5.6}$$

i.e. it is given by the original distribution $P_T(E)$ convoluted by the distribution $P_{evap}(E)$ due to the evaporation process.

There are several other small contributions to the experimentally observed width: a few percent dimers are emitted at the high temperatures attained, the number of collisions with the background gas is small but not

zero. All these effects can be effectively lumped together to produce an effective P_{evap}. As this distribution is quite symmetric, the maxima of $M_T(E)$ and $P_T(E)$ in Eq. 5.6 coincide for temperatures more than 10K above or below the phase transition.

5.3 Canonical or microcanonical data evaluation

It was discussed above that the ensemble of clusters has a canonical distribution of initial energies, but that each single cluster arriving in the laser interaction zone corresponds to a microcanonical ensemble. The question thus arises, which kind of experiment is performed, a canonical or a microcanonical one? In fact neither is performed, but something more fundamental is measured: the distribution $P_T(E)$ of which either a canonical or a microcanonical evaluation can be done.

For a plot of a caloric curve one must know E as a function of the temperature. As $P_T(E)$ has a finite width one must have a prescription how to evaluate this energy from $P_T(E)$. One has two different possibilities: 1) If one uses the mean energy

$$E_{can} = \int E P_T(E) dE \; \Big/ \int P_T(E) dE \tag{5.7}$$

one has a *canonical* situation [34]. One can show analytically, that in this case the canonical caloric curve (Fig. 11d) is a monotonously increasing function [34, 43, 44] and the heat capacity (11f) thus always positive. 2) If one uses the extrema E_{ext} of $P_E(T)$ one has a *micro-canonical* situation. This can be seen by differentiating Eq. 5.1 with respect to the energy. The condition for an extremum of $P_E(T)$,

$$T = (\partial S(E)/\partial E)^{-1} \equiv T_{\mu can} \qquad , \tag{5.8}$$

is identical to the definition of the microcanonical temperature $T_{\mu can}$ as the inverse of the slope of the entropy [34]. Thus, a plot of E_{ext} against the temperature T of the heat bath is identical to the microcanonical caloric curve (Fig. 11c), which is defined as a graph of E against $T_{\mu can}$.

Except near the phase transition, the caloric curve is quite linear and the distributions $P_T(E)$ are thus nearly Gaussians. Maximum and center of $P_T(E)$ are almost at the same energy. This conclusion is not altered by the statistical evaporation process, as the distribution P_{evap} of Eq. 5.6 is also nearly symmetric. Thus canonical and microcanonical caloric curves obtained do not differ from each other within experimental accuracy.

The situation is more complex in the temperature range $\pm$10K around the melting point. The surprising features occurring there are summarized below in part 6.1 and in the caption to Fig. 11. The distributions $P_T(E)$ are asymmetric (see Fig. 11 b, temperatures T_2 to T_4), maximum and mean

are no longer identical, and the two caloric curves differ from each other (see Fig. 11 c and d). Additionally, neither the maximum nor the mean of $P_T(E)$ agree with the maximum of $M_T(E)$ of Eq. 5.6. Experimentally, both caloric curve are smeared out due to the convolution with P_{evap}. For the construction of the caloric curve in Fig. 7 the maxima of the distribution $M_T(E)$ have been followed; a microcanonical curve is thus obtained, averaged by the statistical broadening.

Summarizing this part one can say that one can either make a canonical or a microcanonical evaluation of the data. All caloric curves given here and published earlier have been obtained by following the maxima in data similar to those in Fig. 5. Microcanonical caloric curves are thus obtained, averaged over the distribution $P_{evap}(E)$ of Eq. 5.6. The averaging is only important close to the phase transition, $\pm$ 10 K away from T_{melt} canonical and microcanonical curve are the same within experimental error.

6 Results obtained from the closer look

6.1 Negative heat capacity

There exists a surprising theoretical prediction for a small system: its microcanonical heat capacity can (but must not) become negative. An increase of energy can – under certain conditions – lead to a lower temperature. Every day experience tells us the contrary, if energy is added to a system it will get warmer. But negative heat capacities have since long been known in astrophysics [43, 44], where energy can be added to a star or star cluster which then cools down. A similar effect has been calculated for melting atomic clusters [4, 45] and fragmenting nuclei [35, 46].

Only the positions of the fragment groups have been used so far for the determination of the caloric curves. As discussed elsewhere [47] a negative heat capacity cannot be observed in this case. One thus needs more information, which can be indeed obtained from the measured fragment distributions.

The entropy $S(E)$ of a small system can exhibit a curious structure near a phase transition, a dent with an inverted curvature as shown in Fig. 11. This structure has been predicted by theory and has been observed in many numerical simulations [4–6, 35, 45]. The inverted curvature of the entropy has two interesting consequences 1) The microcanonical caloric curve $T_\mu(E)$ gets a negative slope (colloquially called backbending), which means that the corresponding heat capacity becomes negative. 2) The canonical energy distribution $P_T(E)$ shows a bimodal structure [4–6, 35, 45, 48].

Since $P_T(E)$ is mapped onto the shape of the fragment groups, these should become bimodal, too. An observation of the bimodality would therefore be a direct proof of a negative heat capacity. Fragment distributions were studied in detail for Na^+_{147}, a cluster for which the effect of a nega-

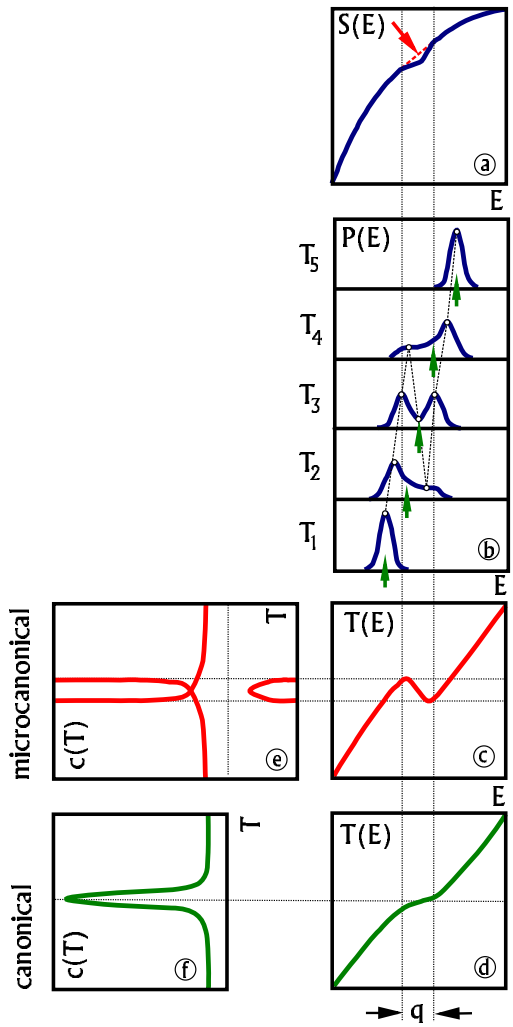

Fig. 11. a) Near a phase transition a small system can show a curious structure in the entropy, a dent where the curvature is negative. This "convex intruder" (arrow) is quite small but has far reaching consequences. b) The energy distributions P(E) become bimodal near the phase transition T_3. c) For the microcanonical caloric curve one has to plot the energy of the extrema of P(E) against the temperature, which results in "backbending" due to the bimodality. d) The canonical caloric curve is a plot of the mean energy [vertical arrows in b)] against the temperature, which gives always a monotonic curve. Its derivative, f) is always positive, while the derivative of the microcanonical curve [e] can become negative.

tive heat capacity can be expected to be particularly pronounced due to its very high latent heat [6, 15, 16]. Unfortunately, the bimodality could not be observed directly, as there are broadening mechanisms in the fragmentation process which just smear out these details. One has to apply a trick which enhances the modulation of the fragment spectra: for a certain photon energy the overlap of adjoining fragment groups produces a pattern which allows one an unambiguous decision whether or not the microcanonical caloric curve shows backbending.

The details of data evaluation [47] are a bit technical and will not be discussed here. One can indeed show that Na^+_{147} has an entropy with an inverted curvature and consequently a negative heat capacity in the energy range of the phase transition. A quantitative estimate for this heat capacity can be obtained from a least square fit [49] to the data: at the melting temperature an increase of the internal energy of Na^+_{147} by 1 eV leads to a concomitant decrease in temperature by about 10K.

How can this negative heat capacity be interpreted? Upon melting, a large system converts added energy completely into potential energy, reducing continuously the fraction of its solid phase. The kinetic energy and thus the temperature remain constant. A small system, on the other hand, tries to avoid partly molten states and prefers to convert some of its kinetic into potential energy instead. Therefore the cluster can become colder, while its total energy increases.

Negative heat capacities have now been found for melting clusters, fragmenting nuclei, and astronomical objects. What do these widely different systems have in common? The answer is that in these systems energy is not an extensive quantity; i.e. if such a system is divided into arbitrary subsystems, the total energy is not simply the sum over the subsystems. The interaction between the subsystems has to be taken into account [34, 44, 50]. For example, in stars it is impossible to neglect the gravity between parts of the system [43, 44]. Similarly in clusters and nuclei the interaction between subsystems is not negligible due to their small size.

6.2 Entropy

The entropy $S(E)$ can be obtained by integrating Eq. 5.8:

$$S(E) = \int dE/T(E) \qquad . \tag{6.1}$$

Inserting the inverse of the measured caloric curve $T = T(E)$, one can calculate the entropy (up to an additional constant) from the experimental data. The result for Na^+_{147} looks like the one given in Fig.11a. The dent is surprisingly small, only about $3{\cdot}10^{-5}$ eV/K at a total value of $S(n = 138, T_{melt}) \approx 15$eV/K. This method is the only experimental one, which allows one to determine entropies for clusters.

Rewriting Eq. 6.1 one obtains:

$$S(T) = \int dT c(T)/T \qquad , \tag{6.2}$$

where c is the heat capacity defined in Eq. 2.1 [7]. The measured caloric curves are piecewise quite linear and the heat capacity thus constant there. This gives a $c \ln T$ dependence of the entropy and for the density of states $\Omega \propto T^c$. As the heat capacity is about proportional to the number of degrees of freedom $(3n-6)$ one sees how dramatically the density of states increases with increasing number n of particles in a cluster.

In principle, one could also say that this experiment measures entropy directly, as the energy distribution $P_T(E)$ produced by the source is just the exponential of the entropy times the Boltzmann factor (see Eq. 5.1), and this $P_T(E)$ is mapped by the fragmentation process onto the mass spectrum. Practically, the convolution integral of Eq. 5.6 cannot be inverted due to numerical noise problems, but outside $\pm$ 10K of T_{melt} it can be solved numerically.

7 Unsolved problems

For several interesting problems there is no or only a partial answer today:

1. How does the caloric curve look at low and very low temperatures? A lot of interesting information is expected there. For bulk matter, the phonon heat capacity goes as T^3 while the electronic one scales as T for a metal, becoming the dominant one at sufficiently low temperature. For finite systems, one has a gap between ground and first excited state both in the electronic and vibrational density of states. Thus both heat capacities must go exponentially to zero for very low temperatures. As the vibrational gap is much smaller than the electronic one, the electronic heat capacity will be exponentially small compared to the vibrational one at very low temperatures, even for metal clusters.

2. Are there other cluster sizes with negative heat capacity near the melting transition? This is expected as many calculations have seen this effect.

3. The experiments have been carried out so far with positively charged sodium clusters. What would be the results for neutral, negatively, or doubly positively charged clusters?

4. How can the method discussed here be generalized to other elements or even molecules? This will not be a problem with the other alkalines. But for many other elements one runs into a problem: The

photon energy must be at least three to four times the dissociation energy D, otherwise the modulation of the mass spectra seen in Fig. 5 and 11 becomes too weak, and no caloric curve can hence be extracted from them. Dissociation energies of several volts are not uncommon, and the necessary powerful lasers are often not available at the required high photon energies. Also they will lead to ionization, further complicating the analysis.

5. Can one study the caloric curve of the liquid to gas transition for a cluster? Experimentally, this is not possible. There seems to be, however, a possibility to construct this curve.

6. Can other types of phase transitions be measured, e.g. the magnetic one, where de Heer and coworkers have published a beautiful first attempt [13]. Unluckily, the ferromagnetic materials have high dissociation energies, and one runs into the problem discussed in point 4 above.

8 Summary and Outlook

The melting of a small finite system in vacuum has been discussed. The experiments have been carried out with positively charged sodium clusters, but many results should be independent of the chemical nature of the element under study and thus be quite general in nature. The main results can be summarized as:

1. The caloric curve of free, mass selected clusters in vacuum has been measured. The measuring process can be divided into two parts:

   - Sodium cluster ions, Na_n^+, are thermalized, which gives them a canonical distribution of internal energies. One cluster size is selected. This prepares a cluster of known temperature T, containing an exactly known number of constituents.
   - The selected cluster is irradiated with a laser, and the distribution of photofragments is measured as a function of the cluster temperature. From this the total internal energy E of the cluster can be determined.

   Knowing E and T, one can construct the microcanonical caloric curve $E = E(T)$, averaged over an experimentally unavoidable broadening.

2. The melting point, and the latent heat of fusion can be directly read off the caloric curve.

3. The melting points of Na_n^+, $55 \leq n \leq 340$:

- are about one third lower than in the bulk,
- they fluctuate by about $\pm$ 50 K,
- the physical origin of fluctuations is not known.

4. The latent heat of fusion shows similar fluctuations as the melting point.

5. The microcanonical heat capacity is negative near T_{melt} for Na^+_{147}. Theory indicates that this should be not an uncommon behaviour for other clusters, but the broadening due to the photofragmentation has so far precluded its observation, save for this one favourable case.

6. The entropy of the size selected cluster can be determined, save near T_{melt}.

There are several other fields of science where similar phenomena are observed or applied. The atomic *nucleus* is a finite system for which phase transitions have been studied intensively. Due to its large zero point motion, the nucleus does not become solid. But it shows a liquid to gas transition, which has interesting similarities to the cluster case [46], i.e. it can have also a negative heat capacity. The determination of energy and temperature are more involved in the nuclear case.

Finally, are there any applications of the size dependence of the melting point of small particles? This plays an important role in the softening and melting of polymers [51]. Even a medical application has recently been proposed [52]. A drug could be encapsulated in or bound to a tiny particle, whose melting point is adjusted via its size to be just above the body temperature. By an external warming of a specific part of the body the particles could be forced to release the medicine exactly there. One can thus have a high drug concentration in some part and a very small one in another part of the body. As all drugs have unwanted side effects, the potential of such a technique would be great.

9 Acknowledgement

Evidently, the work presented results from the cooperative effort of a whole team of people. Contributed have (in alphabetical order): Jörn Donges, Thomas Hippler, Bernd von Issendorff, Werner Kronmüller, Robert Kusche, Ralph Schlipper, and Martin Schmidt. Financial support came from the Deutsche Forschungsgemeinschaft through SFB 276.

References

[1] P. Pawlow, Z. Phys. Chem. 65 1 (1909)

[2] S.L. Lai, J.Y. Guo, V. Petrova, G. Ramanath, and G.L. Allen, Phys. Rev. Lett. 77 99 (1996)

[3] S.Berry *Scientific American* 263 50 (August 1990)

[4] P. Labastie and R.L.Whetten, Phys. Rev.Lett. 65 1567 (1990)

[5] C. L. Cleveland, U. Landman, T. G. Schaaf, M. N. Shafigullin, P. W. Stephens, R. L. Whetten, Phys. Rev. Lett.79 1873 (1997)

[6] F. Calvo and F. Spiegelmann, J.Chem. Phys. 112 2888 (2000)

[7] It is not necessary to differentiate between heat capacity of constant volume or pressure, as these are very nearly the same for a solid or liquid.

[8] M.Yu.Efremov et al, Phys. Rev. Lett. 85 3560 (2000)

[9] U. Buck and I. Ettischer, J. Chem. Phys. 100 6974 (1994)

[10] U. Even, N. Ben–Horin, and J.Jortner, Phys. Rev. Lett. 62, 140 (1989)

[11] T.P. Martin, Phys. Rep. 273 199 (1996)

[12] J.W. Hovick and L.S. Bartell, J. Mol. Struct. 413 615 (1997)

[13] A. Hirt, D. Gerion, I.M.L. Billas, A. Châtelain. and W.A. de Heer, Z. Phys. D40 160 (1997)

[14] M. Schmidt, R. Kusche, W. Kronmüller, B. v. Issendorff, and H. Haberland, Phys. Rev. Lett. 79, 99 (1997)

[15] M. Schmidt, R. Kusche, B. v.Issendorff, and H. Haberland, Nature 393 238 (1998)

[16] R. Kusche, Th. Hippler, M. Schmidt, B. v. Issendorff, and H. Haberland, Eur. Phys. J. D9 1 (2000)

[17] M.Schmidt et al., in *The Physics and Chemistry of Clusters* Proceedings of Nobel Symposium 117, (World Scientific, Singapore, 2001), pp. 326.

[18] G. Bertsch, Science 277 1619 (1997)

[19] R. S. Berry, Nature 393 212 (1998)

[20] See chapter 3.2 of [53]

[21] M.F.Jarrold, part 2.7 of [53]

[22] A. Aguado, J.M. Lopez, J.A. Alonso and M.J. Stoll, J.Chem.Phys. 111 6026 (1999)

[23] A. Rytkonen, H. Hakkinen, M. Manninen, Phys. Rev. Lett. 80 3940 (1998)

[24] N. Ju and A. Bulgac, Phys. Rev. B48 2721 (1993)

[25] A. Aguado, J. M. Lopez, J. A. Alonso, and M. J. Stott, J. Phys. Chem. B105, 2386 (2001)

[26] Y.J. Lee, E.–K. Lee, S. Kim, and R.M. Nieminen, Phys. Rev. Lett. 86, 999 (2001)

[27] J. Farges, M.F.de Feraudy, B.Raoult, and G. Torchet, Surf. Science 106, 95 (1981)

[28] A. A. Shvartsburg and M. F. Jarrold, Phys. Rev. Lett. 85, 2530 (2000)

[29] H. Haberland, Physics World, December 2000, page 27

[30] Th. Bachels, H.–J. Güntherodt, R. Schäfer, Phys. Rev. Lett. 85, 1250 (2000)

[31] R. Kofman, P. Cheyssac, and F. Celestini, Phys. Rev. Lett. 86, 1388 (2001)

[32] S.Krückeberg, S.Schoos, M.Maier–Borst, and J.H. Parks, Phys. Rev. Lett., 85, 4494-4497 (2000)

[33] H. Haberland, B.v.Issendorff, Th.Kolar, H.Kornmeier, Ch.Ludewigt, and A.Risch, Phys.Rev.Lett.67, 3290 (1991); H. Haberland, B.v.Issendorff, Ji Yufeng, and Th.Kolar, Phys.Rev.Lett. 69, 3212 (1992)

[34] Landau–Lifshitz, Statistical Physics, Vol. 5 of *Course of Theoretical Physics*, Pergamon Press, London – Paris 1958

[35] D. H. E. Gross, Rep. Prog. Phys. 53, 605 (1990)

[36] A.Hüller, Z.Phys. B93, 401 (1994)

[37] R. Schlipper, R. Kusche, B. von Issendorff, H. Haberland, Appl. Phys. A72, 255 (2001), and PhD thesis R. Schlipper unpublished

[38] See the contribution of G. Bertsch in this book

[39] M. Brack, Rev. Mod. Phys. 65 677 (1993)

[40] W. de Heer, Rev. Mod. Phys. 65 611 1993

[41] H. Haberland in *Metal Clusters* W. Ekardt, ed. J.Whiley 1999

[42] Mainly atoms are evaporated but also about 3% of dimers. This does not change any conclusions discussed here, it only leads to an additional broadening of the mass spectra.

[43] W. Thirring, Z. Phys. 235 339 (1970)

[44] D. Lynden–Bell, Physica A263 293 (1999)

[45] M. Bixon and J. Jortner, J. Chem. Phys. 91 (3), 1631 (1989)

[46] M. D'Agostino *et al.*, Phys.Lett. B473 219 (2000)

[47] M. Schmidt, R. Kusche, Th. Hippler, J. Donges, W. Kronmüller, B. v. Issendorff, and H. Haberland, Phys. Rev. Lett. 2001

[48] A macroscopic system avoids the inverted curvature by phase separation, i.e. being partly liquid, partly solid, as described by the well known van Hove construction [35, 43,44,50]. This is not advantageous for a small system, due to the large percentage of atoms at a liquid/solid interface.

[49] M.Schmidt et al., unpublished results

[50] L. van Hove, Physica 15 951 (1949)

[51] G. Strobl, Eur. Phys. J. E3, 165 (2000)

[52] K. Westesen, Colloid. Polym. Sci. 278 608 (2000)

[53] *Clusters of Atoms and Molecules I* Springer Series in Chemical Physics Vol. 52 (H.Haberland, ed.), Springer 1994